Available online at www.sciencedirect.com
SCIENCE DIRECT®
Ocean Modelling 9 (2005) 133–150
Ocean Modelling
www.elsevier.com/locate/ocemod

A wetting and drying scheme for POM

Lie-Yauw Oey *

Princeton University, AOS, Sayre Hall, Forrestal Campus, Princeton, NJ 08544, USA

Received 7 May 2004; received in revised form 10 May 2004; accepted 3 June 2004
Available online 2 July 2004

Abstract

In shallow-water models, wetting and drying (WAD) are determined by the total water depth $D = 0$ for 'dry' and >0 for 'wet'. Checks are applied to decide the fate of each cell during model integration. It is shown that with bottom friction values commonly used in coastal models, the shallow-water system may be cast into a Burger's type equation for D. For flows dominated by D (i.e. $|\nabla D| \gg |\nabla H|$, where $H(x, y)$ defines topography) a non-linear diffusion equation results, with an effective diffusivity that varies like D^2, so that 'dry' cells are regions where 'diffusion' is very small. In this case, the system admits $D = 0$ as part of its continuous solution and no checks are necessary. For general topography, and/or in the case of strong momentum advection, 'wave-breaking' solution (i.e. hydraulic jumps and/or bores) can develop. A WAD scheme is proposed and applied to the Princeton Ocean Model (POM). The scheme defines 'dry' cells as regions with a thin film of fluid O (cm). The primitive equations are solved in the thin film as well as in other regular wet cells. The scheme requires only flux-blocking conditions across cells' interfaces when wet cells become dry, while 'dry' cells are temporarily dormant and are dynamically activated through mass and momentum conservation. The scheme is verified against the above-mentioned diffusion and Burger's type equations, and tested also for one and two-dimensional channel flows that contain hydraulic jumps, including a laboratory dam-break problem.

Keywords: Wetting and drying; Dam-break; Flood and ebb; Princeton ocean model

1. Introduction

Wetting and drying (WAD) is a common and important phenomenon of the coastal ocean. They occur in low-lying coastal zones and also in embayment and inlets. Strong winds and/or

* Tel.: +1-609-258-5971; fax: +1-609-258-2850.
E-mail address: lyo@princeton.edu (L.-Y. Oey).

1463-5003/$ - see front matter © 2004 Published by Elsevier Ltd.
doi:10.1016/j.ocemod.2004.06.002

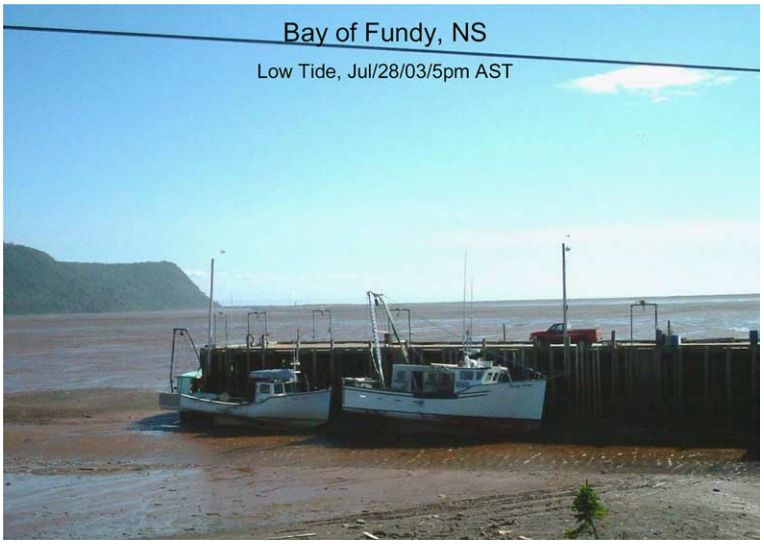

Fig. 1. An example of drying in the Bay of Fundy, Nova Scotia. This photo was taken at a small village located on the eastern shore of the Bay at the indicated time. Local commercial and recreational activities are often timed to the periodic rhythm of the wetting and drying phase of the bay.

tides can cause flooding and subsequent drying. In bays and inlets with extreme tides, such as in the Bay of Fundy and the Cook Inlet, WAD makes up an essential rhythm of life for the local people (Fig. 1).

The Princeton Ocean Model (POM; Mellor, 2002) is a widely used ocean model with a terrain-following sigma-coordinate system in the vertical and an orthogonal curvilinear coordinate system in the horizontal. Because of these features and the fact that the model solves for the sea-level (tides) directly, POM is particularly suited for coastal ocean simulation. Indeed, one of the earliest applications of POM was to simulate tides and their interaction with (river) buoyancy-driven flows in a bay (Oey et al., 1985). In view of the common occurrences of WAD in coastal oceans, it seems surprising that a WAD scheme has not been implemented in POM. The Minerals Management Service (MMS) of the US Department of Interior has sponsored a two-year study (2003–2005; through Princeton University), to develop and test WAD in POM. The goal is to build a WAD scheme that is robust, and that works in tandem with, and extends other existing features of POM onto near-coast regions where WAD processes may prevail (Fig. 2). These other POM features simulate scales ranging from those existing in the deep basin (meso-scale eddies and larger) to slope, shelf and near-coast circulation (wind and rivers). (Recent applications of these larger-scale circulation can be found in Oey and Lee, 2002; Ezer et al., 2003; Oey et al., 2003; Wang et al., 2003; Fan et al., 2004; Oey and Zhang, in press; Oey et al., 2004.) This paper reports the initial development and testing of the WAD scheme in POM. For this purpose, WAD processes in idealized one- and two-dimensional channels are used to illustrate the scheme. A modest objective is to check the accuracy of the scheme against (semi-) analytic WAD solutions (in some limit to be detailed), and also against laboratory data.

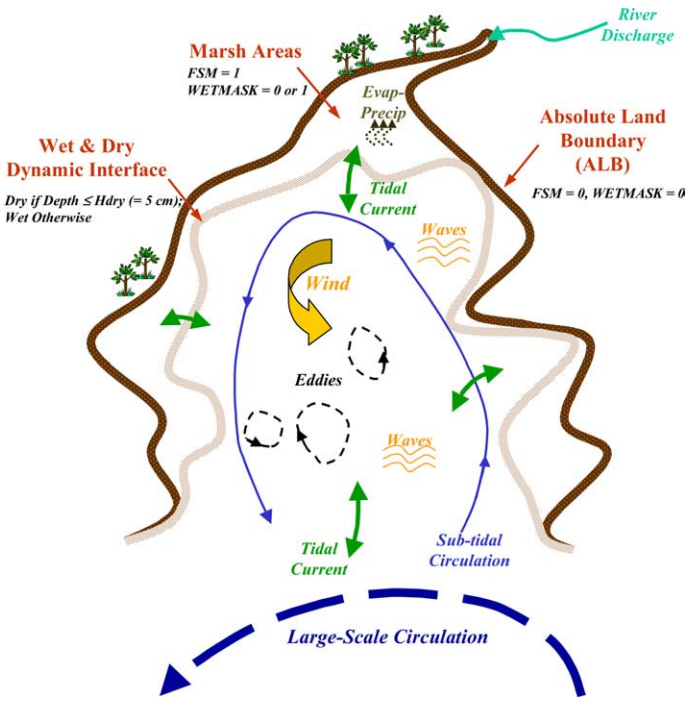

Fig. 2. Schematic of a coastal ocean region that can be flooded and drained (dried) by water-level variations from the open ocean, and the various definitions as discussed in text. In addition to wetting and drying, shown here are also processes of various spatial and temporal scales that can be included in POM. The surface waves part is also a new initiative in POM (Mellor, 2003).

2. A wetting and drying scheme

A number of WAD schemes have been implemented in coastal models. In oceanographic literature, the readers are referred to Flather and Hubbert (1990), Casulli and Cheng (1992), and more recently Ji et al. (2001) for comprehensive summaries. WAD implementations have been routine (and essential) in hydraulic modeling for quite some time (Stelling et al., 1986; Balzano, 1998, and references quoted therein). Coastal engineers routinely deal with rapidly varying WAD processes, including flow expansion, hydraulic jumps and other phenomena of importance for practical designs. A common theme in all the implementations is to invoke blocking and de-blocking conditions at cells' interfaces, for example setting flow across the interface to zero when the water depth D becomes shallower than a pre-assigned depth, $H_{\rm dry} \approx O$ (cm). We give here a simple WAD scheme based on a similar concept but taking advantage also of the POM structure.

In POM (without WAD), a two-dimensional mask, FSM, is used such that FSM = 1 at water cells and FSM = 0 on land cells. POM uses FSM to facilitate the zero-flux conditions across solid boundaries. To implement WAD, we first define an *absolute* land boundary (ALB) over which water can never spill. This is accomplished by making the modeled region sufficiently large to include on its coastal side the highest elevated land points that are *always* 'dry'. Thus FSM = 0 on and landward of the ALB delineated by the thick curve in Fig. 2. Seaward of the ALB, we set

FSM = 1 always, but here cells can be wet or dry. We define (for coding convenience) a separate time-dependent mask, "WETMASK", such that WETMASK = 0 where FSM = 0, but seaward of the ALB where FSM = 1, WETMASK = 0 at dry cells and = 1 at wet cells. In Fig. 2, these cells are schematically shown to be the "marsh" areas that lie between the ALB and the "wet and dry" dynamic interface. But they can be (and are) in general anywhere seaward of the ALB. Whether or not a cell is dry is determined through mass and momentum conservation in that cell as well as in the neighboring cells. To invoke these conservation laws, we define dry cells as having a film of fluid of thickness $H_{\rm dry} = 5$ cm and solve (POM's) primitive equations in these cells as well as in other regular water cells. (Note that because of POM's algorithmic structure, the code requires a non-zero water depth at all cells.) At each time step, D at cells' interfaces (where flow velocities are defined in the *C-grid* used in POM) are checked, and the velocity is set to zero if the D drops below $H_{\rm dry}$. In this way, a wet cell becomes dry if there is excessive flow divergence from that cell, and a dry cell becomes wet if there is sufficient convergence. Divergences and/or convergences depend on dynamics, such as pressure gradients, friction etc. across cell's interfaces.

In summary, the new POM-WAD defines absolute land areas over which water can never spill. Other cells can be wet or dry. By assigning a thin (O (cm)) but finite film of fluid in the dry cells, they can be solved together with other water points, and conservation of mass and momentum decides their temporal evolution (i.e. whether or not they become wet or dry in the next time step etc.). Conditions do need to be imposed at cells' interfaces, but these are very simple requiring only that velocities are set zero if water depth drops below the pre-assigned thickness of the thin film. Note that in the original POM, there are always cells seaward of the ALB that are forced to

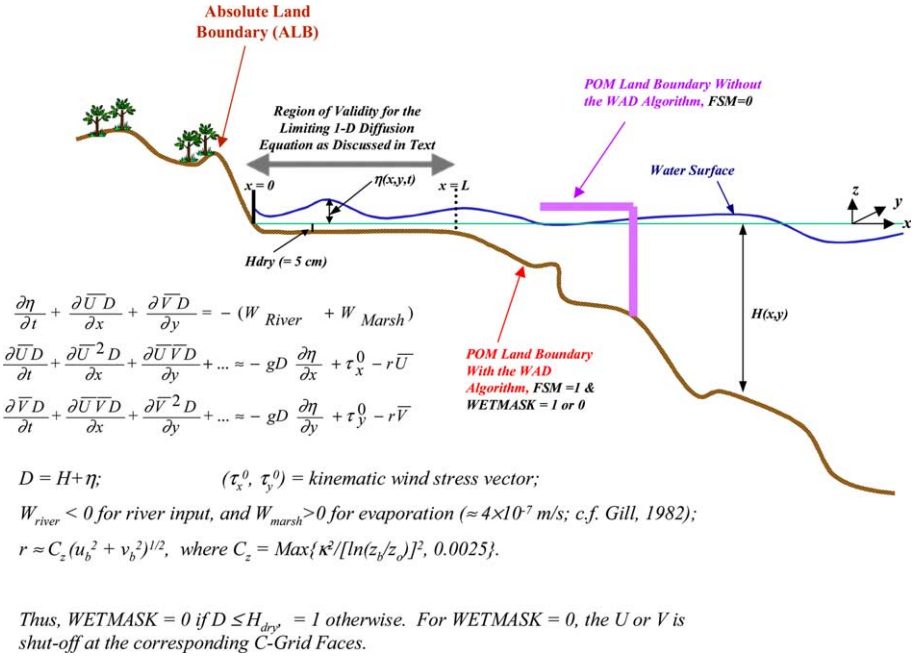

Fig. 3. An illustration of the wetting and drying algorithm in a cross-shore vertical section and using the POM's depth-averaged equations. See text for details.

be permanently land (FSM = 0) or wet (FSM = 1) by a somewhat arbitrary redefinition of the topography; i.e. by 'shaving' the cell or 'dredging' it (Fig. 3). This restriction is now removed in POM-WAD. In examples given below, POM-WAD works well for bottom friction values commonly used in coastal models (reason to be given shortly). When simulating hydraulic jumps or propagating bores, it will be found necessary to modify the scheme so that "D" is solved using a positive-definite advection scheme, for otherwise excessive oscillations can lead to numerical instability (see below).

3. One-dimensional channel examples

The above implementation is illustrated in Fig. 3, which shows the situation for the depth-averaged equations. These are the same as the 'external-mode' equations used in POM except that the baroclinic terms are omitted and the depth-averaged velocities $(\overline{U}, \overline{V})$ are used in the bottom friction terms. Also, the W_{River} simulates river input (Oey, 1996) and W_{Marsh} lumps together evaporation minus precipitation and/or absorption by mud and/or vegetation. One may imagine an initial-value problem in which tide (for example) propagates onto an initially dry marsh-land (FSM = 1 and WETMASK = 0) (or extreme tide of large amplitude propagating onto land). Grid cells over marsh then 'feels' the pressure gradient (since FSM = 1) exerted by the tide and in time becomes overrun by water (WETMASK = 1). When the tide recedes, the opposing pressure gradient can produce dry cells. This section illustrates and checks the accuracy of POM-WAD with simple one-dimensional channel cases.

3.1. Simple considerations

Consider a one-dimensional channel $(0, L)$. Let $x = 0$ be the grid cell that represents the ALB, and $x = L$ be the seaward grid cell onto which the tide propagates from open ocean $x > L$. The channel's bottom depth is conveniently defined as $H_{\text{d}}(x)$ meters (always >0) below some datum line, say a horizontal line that originates from (the lowest) point of the absolute land boundary. In the notations of Fig. 3, $H_{\text{d}} = H + \text{constant}$, where $H(x)$ (also >0) is bottom depth below the mean sea level. We assume zero surface inputs (winds, river and/or evaporation–precipitation) and no absorption by mud and vegetation. The governing equations in terms of D and $\overline{U}$ are (Fig. 3):

$$\frac{\partial D}{\partial t} + \frac{\partial \overline{U} D}{\partial x} = 0 \tag{1a}$$

$$\frac{\partial \overline{U} D}{\partial t} + \frac{\partial \overline{U}^2 D}{\partial x} = -gD\left(\frac{\partial D}{\partial x} - \frac{\partial H}{\partial x}\right) - \frac{r}{D}\overline{U} D \tag{1b}$$

In the case when the $\frac{\partial \overline{U}^2 D}{\partial x}$ term on the LHS of (1b) may be assumed small, eliminating $\overline{U} D$ and setting $r/D \approx r/H_0$, where H_0 is a constant (some average of D, say), gives:

$$\frac{\partial^2 D}{\partial t^2} + \left(\frac{r}{H_0}\right)\frac{\partial D}{\partial t} \approx \frac{\partial}{\partial t}\left(gD\frac{\partial (D - H)}{\partial x}\right) \tag{2}$$

subjected to the following boundary conditions,

$$\frac{\partial(D-H)}{\partial x}=0 \quad \text{at } x=0 \tag{3a}$$

$$D=E(t) \quad \text{at } x=L \tag{3b}$$

and some initial profile of D,

$$D=F(x) \quad \text{at } t=0 \tag{4}$$

Eq. (3a) is the zero-flux condition at the left-side solid boundary, and (3b) specifies water-level fluctuation at the right-side open ocean, assumed to be $E(t)$ ($=D_0 e^{i\omega t}$, say, i.e. sinusoidal with frequency ω and amplitude D_0).

It is useful to examine some limiting cases. When $r=0$ and $H=$ constant, Eq. (2) reduces to the familiar linearized wave (e.g. tidal) equation. If on the other hand the $\frac{\partial^2 D}{\partial t^2}$ term is small compared to the friction term, Eq. (2) becomes parabolic. The condition for friction to dominate is, from Eq. (1b):

$$\mathrm{Min}\left(\frac{r}{D\omega},\frac{rl}{\overline{U}D}\right)\gg 1 \tag{5}$$

where l is the spatial scale (and ω the frequency) of the motion. Typical values are $r\approx 10^{-4}$–10^{-3} m/s (in POM, and also Balzano, 1998), $\omega\approx 10^{-4}\ \mathrm{s}^{-1}$ (e.g. M_2 tide), $D=O(1)$ m, $|\overline{U}|=O(1)\ \mathrm{m\,s}^{-1}$, and $l\approx 100'\mathrm{s\,km}$ for tides. Thus, except when $l\approx 10'\mathrm{s\,km}$ and less (hydraulic jumps and/or bores), the second of (5) is usually satisfied and the non-linear momentum advection term may be dropped. The requirement that the first of (5) is also satisfied is not crucial to WAD processes, but it leads to useful insights. Thus, if we drop terms on the left hand side of (1b), we obtain (upon eliminating $\overline{U}D$ from (1a) and (1b) as before) the following equation for D: [1]

$$\frac{\partial D}{\partial t}\approx\frac{\partial}{\partial x}\left(\frac{gD^2}{r}\left(\frac{\partial D}{\partial x}-\frac{\partial H}{\partial x}\right)\right) \tag{6}$$

Except for the use of $r/D\approx r/H_0$ in the derivation of (2) and the presence of $\frac{\partial^2 D}{\partial t^2}$ term, Eqs. (2) and (6) are identical. Expanding (6), we obtain:

$$\frac{\partial D}{\partial t}+\left(\frac{2gDH_x}{r}\right)\frac{\partial D}{\partial x}=\frac{\partial}{\partial x}\left(\frac{gD^2}{r}\frac{\partial D}{\partial x}\right)-\frac{gD^2}{r}\frac{\partial^2 H}{\partial x^2} \tag{7}$$

a non-linear advection–diffusion (Burger's type) equation for D, with a source term. The 'advection velocity' is $(2gDH_x/r)$, the sign of which solely depends on the sign of bottom slope H_x. The 'diffusivity' (gD^2/r) is non-linear but positive definite. The source term is proportional to H_{xx}; it is a sink for convex topography $H_{xx}>0$ (i.e. a 'hill'), and a source for concave topography $H_{xx}<0$ (i.e. a 'bowl'). [2] Physically, flow over a concave bottom tends to accumulate and vice versa for a convex bottom. To interpret the 'advective' and 'diffusive' terms, consider rising sea level (i.e. flood) at $x=L$ that propagates into an initially empty channel with $H_x>0$. The 'advective' term $(2gDH_x/r)(>0)$ is proportional to the component of gravity (gH_x) of fluid column D in the down-

[1] The Appendix A gives the corresponding two-dimensional case.

[2] It is clear from its derivation that the 'source' term coexists with the 'advective' and 'diffusion' terms, in other words, Eq. (6) gives $D=H+$ *constant* for a motionless fluid, hence $\partial D/\partial t=0$.

slope direction, and it tends to stretch sea level down the channel. The stretching tends to flatten sea level, more so for larger D and smaller r, so that the channel fills up more uniformly during flood. The stretch is less for larger r, and sea-level tilts upward with increasing x (i.e. larger friction requires stronger pressure gradient). For ebbing (again initiated at $x = L$) of an initially filled channel, it is possible that $D_x < 0$ at some x, and the reduced stretching with x can lead to a 'wave-breaking' solution. For more complex H with non-zero curvature, the 'advective' term varies (with x) and can change sign, and Eq. (7) suggests the possibility of a 'wave-breaking' solution (flood or ebb into a bowl-shaped basin).

The 'diffusive' term is best interpreted for $H_x = 0$, in which case (7) reduces to a pure diffusion equation:

$$\frac{\partial D}{\partial t} = \frac{\partial}{\partial x}\left(\frac{gD^2}{r}\frac{\partial D}{\partial x}\right) \tag{8}$$

The same equation is obtained from (6) by invoking $|\nabla D| \gg |\nabla H|$. The resulting system, Eqs. (8), (3) and (4), forms a well-posed initial/boundary-value problem that admits WAD processes (i.e. D can be zero) as part of a continuous solution. In such a system, it is *not* necessary to invoke any blocking or de-blocking condition. An example would be flooding and ebbing of a shallow channel $(0, L)$ connected to a deeper open ocean at $x = L$ (Fig. 3). The rise and fall of sea level at $x = L$ are 'diffused' into the channel in a manner dependent on the non-linear (but positive definite) 'diffusivity coefficient' gD^2/r. Using the heat-conduction analogy (Carslaw and Jaeger, 1959), the diffusive penetration distance, L_{pd} say, at a given time t is proportional to $D(g/r)^{1/2}$. There is an asymmetry between flooding and ebbing. Since $D \to 0$ at $x = L$ when the open-ocean sea-level falls, the 'ebbing' signal diffuses very slowly into the channel. The opposite would be true for flooding, when we can expect more rapid sea-level rise ('diffusion' of D) and intrusion of open-ocean water into the channel. Note also that the L_{pd} also varies with the bottom drag coefficient, like $r^{-1/2}$. Larger friction retards flow, and limits flooding or ebbing. As $r \to 0$, Eq. (8) is invalid and (2) reverts to the linear wave equation.

Eq. (2), or Eq. (7) with the frictional restriction, and (3) and (4) are easily solved using finite differences (Richtmyer and Morton, 1957). Some solutions will now be given and compared with those obtained directly from POM-WAD.

3.2. Testing POM-WAD

The solutions to the above Eq. (2) with boundary/initial conditions (3) and (4) provide excellent checks for the accuracy of the WAD algorithm in POM (i.e. with WETMASK and flux-blocking conditions etc.), In cases for which condition (5) is satisfied, the solutions are further confirmed with those obtained from Eq. (7) or (8). We first test the case of a flat-bottom channel, next a linear sloping bottom, then a channel with a step, and finally a more complex (convex and concave) bottom.

3.2.1. A flat-bottom channel

The (numerical) solutions to Eq. (8) with (3) and (4) are shown in Fig. 4 as solid curves (initial profile of D is shown dotted and is labeled "0.0") for (a) ebbing and (b) flooding. Two grid sizes, $\Delta = 1.25$ and 0.625 km were tested and the results were virtually identical. The cases for $\Delta = 0.625$

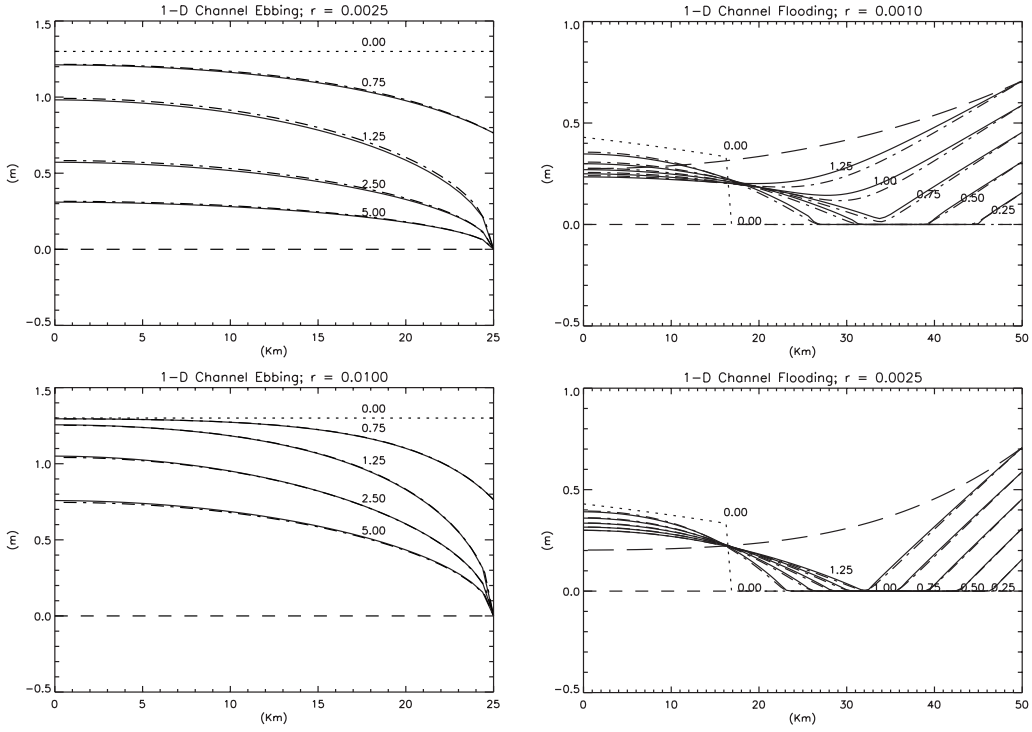

Fig. 4. (a) Left panels: An ebbing simulation in a channel of length 25 km, closed at the western end and open in the east. Water level is lowered to 0 at the east over a period of 1.25 days following a cosine time variation, and kept at 0 for the remaining period through day 5. Plotted are curves of the water level at various times, solid: solution of diffusion equation; dash-dot: POM-WAD solution. Upper panel is for $r = 2.5 \times 10^{-3}$ m s^{-1} and lower panel for $r = 10^{-2}$ m s^{-1}. Numbers on selected curves indicate times in days. For example, the curve for initial water level is indicated by "0.0". (b) Right panels: A flooding simulation into an initially partially wet (western third) channel of length 50 km, closed at the western end and open in the east. Water level is raised at the east following a half-sine time variation, to a maximum of 1 m over a 2.5-day period and kept at 1 m thereafter. Plotted are curves of the water level at various times, solid: solution of diffusion equation; dash-dot: POM-WAD solution. Upper panel is for $r = 10^{-3}$ m s^{-1} and lower panel for $r = 2.5 \times 10^{-3}$ m s^{-1}. Numbers on selected curves indicate times in days. For example, the curve for initial water level is indicated by "0.0". Long dashed curve shows the solution at $t = 1.25$ day when the diffusivity is linearized using $D = 1$ m.

km are shown here. The solutions obtained from POM-WAD are shown as dash-dot curves. In Fig. 4a (left panels) the channel's length is $L = 25$ km and is initially filled with water of uniform depth $D_0 = 1.3$ m. The sea level is then lowered at $x = L$ to $D = 0$ over 1.25 days, and kept at '0' through day 5:

$$\begin{aligned} E(t) &= D_0 \cos(\omega t), \quad 0 \leqslant t < 1.25 \text{ days} \\ &= 0, \qquad\qquad 1.25 \text{ days} \leqslant t \leqslant 5 \text{ days} \end{aligned} \tag{9}$$

where $\omega = 2\pi/(5 \text{ days})$. The solutions are shown for two different $r = 2.5 \times 10^{-3}$ and 10^{-2} s^{-1}. These values of r and ω are chosen so that condition (5) is satisfied, and the solutions to (8) and (2)

are indistinguishable. It is seen that the effect of drying at $x = L$ 'diffuses' slowly into the channel as the channel empties, and that the emptying is faster for smaller r. A boundary layer appears near $x = L$, and it slowly vanishes with time. As the open-ocean (i.e. in region $x > L$) sea-level drops below the channel's mouth, the shallow channel flow with friction takes longer time to adjust, and fluid is drained slowly. An illustration of this phenomenon when flow in the 'open ocean' is also considered will be given shortly.

In Fig. 4b (right panels), the channel's length is $L = 50$ km and is initially partially filled with water as shown by the dotted curve: wet on the western third of the channel and dry on the eastern two-thirds. The sea level is then raised at $x = L$ to $D = 1$ m over 2.5 days, and kept at 1 m through day 5:

$$\begin{aligned} E(t) &= D_0 \sin(\omega t), \quad 0 \leqslant t < 2.5 \text{ days} \\ &= 1, \qquad\qquad 2.5 \text{ days} \leqslant t \leqslant 5 \text{ days} \end{aligned} \tag{10}$$

where now $\omega = 2\pi/(10 \text{ days})$. Fig. 4b shows that at the initial wet–dry transition ('jump') at $x = L/3$, the jump spreads by virtue of 'diffusion' of D, and that the flooding intrusion from $x = L$ also diffuses into the channel. Since the D for the two different r is of the same order of magnitude, the wetting penetration distance L_{pd} at a given time t is approximately proportional to $(g/r)^{1/2}$. Thus L_{pd} increases by about 60% as r is decreased by a factor of 2.5 from $r = 2.5 \times 10^{-3}$ m s^{-1} (lower panel) to $r = 10^{-3}$ m s^{-1} (upper panel). Compare, for example, the curves labeled '0.5' in Fig. 4b, which shows an $L_{\text{pd}} \approx 11$ km for $r = 10^{-3}$ m s^{-1}, and 7 km for $r = 2.5 \times 10^{-3}$ m s^{-1}. Fig. 4b also shows a curve at $t = 1.25$ day (long dashes) for which the diffusivity in Eq. (8) is linearized with $D = 1$ m. The result (and also at other times, and other values of lienarized D; not shown) shows poor agreement with the non-linear formulation. Non-linear diffusivity is crucial as it allows simulation at dry locations where diffusion is zero.

Fig. 4a and b also show the corresponding POM-WAD solutions. The agreements with solutions of the non-linear diffusion Eq. (8) (or (2)) are good. As one would expect, better agreements are obtained with larger friction. For these frictional solutions, a very small $H_{\text{dry}} = 10^{-4}$ m is used (to mimic as close as possible the continuous solution of (8) that contains $D = 0$) without causing undue numerical problems in the POM-WAD algorithm. The solutions with $H_{\text{dry}} = 5$ cm are similar except that the dry-wet transitions (e.g. in Fig. 4b) are smoothed.

3.3. A channel with linear sloping bottom

We next consider the case $H(x) = 10x/L$, i.e. depth is zero at $x = 0$ where the channel is again closed (i.e. an ALB point), and linearly increases to $D_0 = 10$ m at the open-ocean end $x = L$. The channel is initially dry, $F = 0$ in (4). Water level at $x = L$ is then sinusoidally raised and lowered over a period of 0.5 day ($\approx M_2$ period):

$$E(t) = D_0 \sin(\omega t), \quad (n-1) \times 0.5 \text{ day} \leqslant t < n \times 0.5 \text{ days} \tag{11}$$

where $n = 1, 2, 3, \ldots$, and $\omega = \pi/(0.5 \text{ days})$. Fig. 5 shows the POM-WAD inviscid result for the first cycle ($n = 1$) in terms of water level and velocity (colored) at the ten indicated times over the

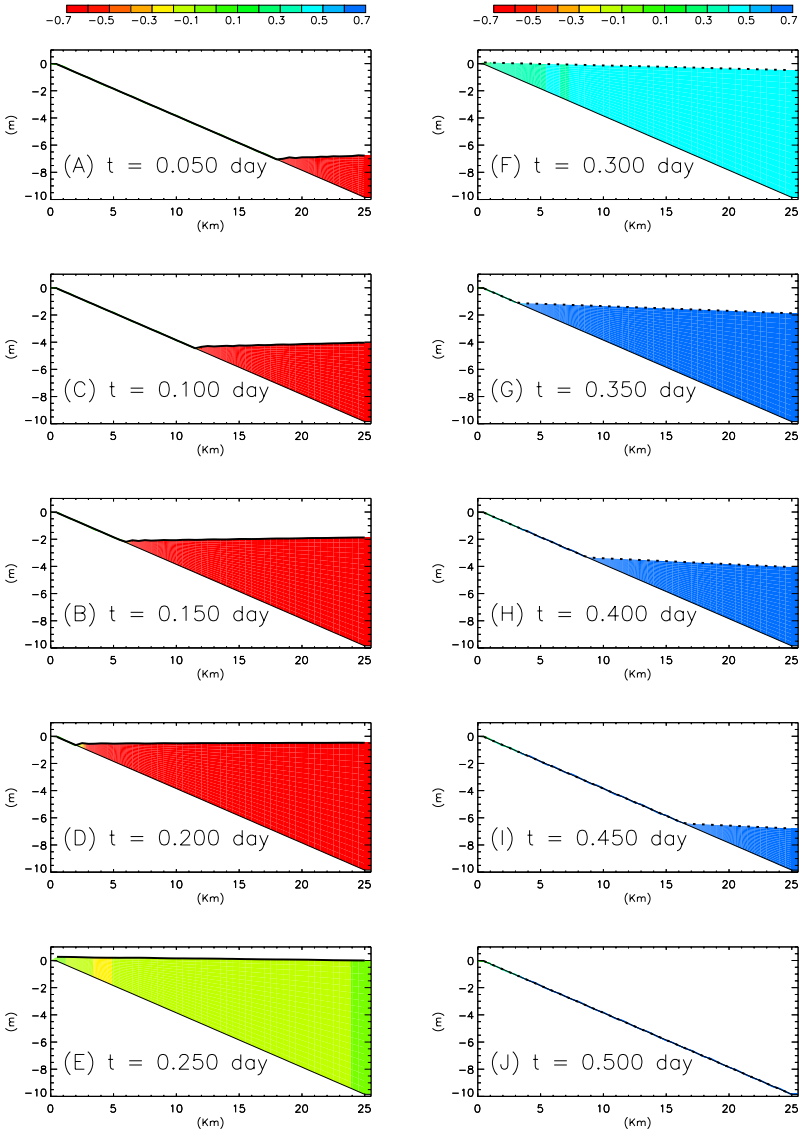

Fig. 5. Flooding (wetting) and ebbing (drying) POM-WAD simulation in a channel with linear sloping bottom topography, closed at left ($x = 0$) and open at right ($x = L = 25$ km) where rising and falling sea level is specified over a 0.5 day period. Shown are water level and velocity (in color scale in m/s given on top) at the indicated times. Left panels (A–E) are flood and right panels (F–J) are ebb. The friction coefficient $r = 0$.

cycle, and Fig. 6 shows the corresponding results for $r = 10^{-2}$ m s^{-1} case. In the inviscid case (Fig. 5), sea-level rises (falls) more or less uniformly through the channel, with only slight tilts. This is as expected since inviscid signal travels fast as $(gD)^{1/2}$, and there is little delay between seaward and landward sea level.The channel fills up at end of each half cycle and empties at end of the cycle—i.e. there is no residual water. It can be seen that POM-WAD produces smooth transitions from

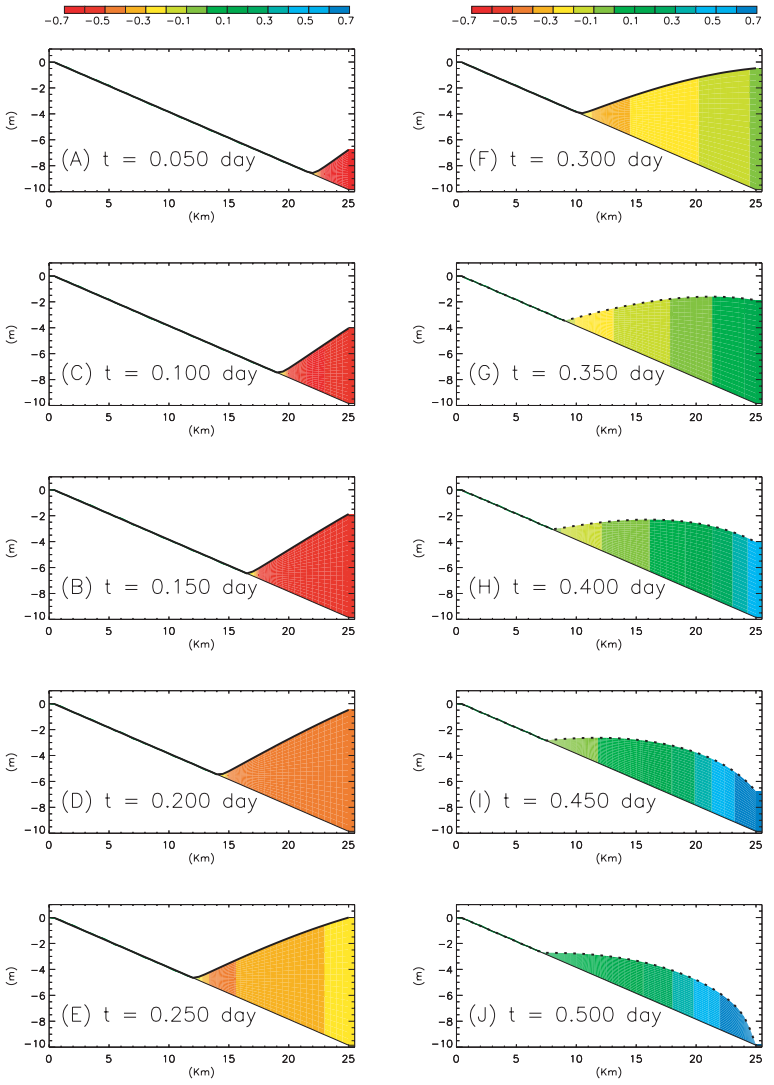

Fig. 6. Flooding (wetting) and ebbing (drying) POM-WAD simulation in a channel with linear sloping bottom topography, closed at left ($x = 0$) and open at right ($x = L = 25$ km) where rising and falling sea level is specified over a 0.5 day period. Shown are water level and velocity (in color scale in m/s given on top) at the indicated times. Left panels (A–E) are flood and right panels (F–J) are ebb. The friction coefficient $r = 10^{-2}$ m/s.

dry to wet during flood and wet to dry during ebb. I have checked the model to $n = 5$ cycles and the solution repeats (not shown).

The solution is quite different for the frictional case (Fig. 6). Its behavior matches that predicted by Eq. (7). At flood, sea-level tilts steeply as pressure gradient is required to balance friction. In this case, 'stretching' effect due to the 'advective' term in (7) is less than the inviscid case (Fig. 5), and also less than the case with smaller r (not shown). During ebb, as water depth at $x = L$ drops

below that inside the channel, water level becomes more convex as its thickest portion is 'stretched seaward' more, and a 'breaking-wave' solution begins to form near the end of the cycle near $x = L$. This results in a convex pool of water being left behind in the channel at the end of ebb. The result is also simply explained by the well-known fact that, with friction, currents lag tide (e.g. Proudman, 1953; in the large friction limit the two terms on the right hand side of (1b) balance), and flooding currents still exist near the head of the channel after sea level at the mouth falls (Fig. 6F and G). Note that in the frictional case, solution for later cycles ($n > 1$) would differ from the first cycle ($n = 1$; because of the convex pool left at the end of cycle 1), but the solutions repeats for $n \geqslant 3$ (not shown).

Fig. 7 checks the above POM-WAD solutions (dash-dot curves) against those computed from (7) (solid curves) for $r = 2.5 \times 10^{-3}$ m s^{-1} (upper panel) and $r = 10^{-2}$ m s^{-1} (lower panel). Plotted are water depths D at the indicated times. The agreements are good.

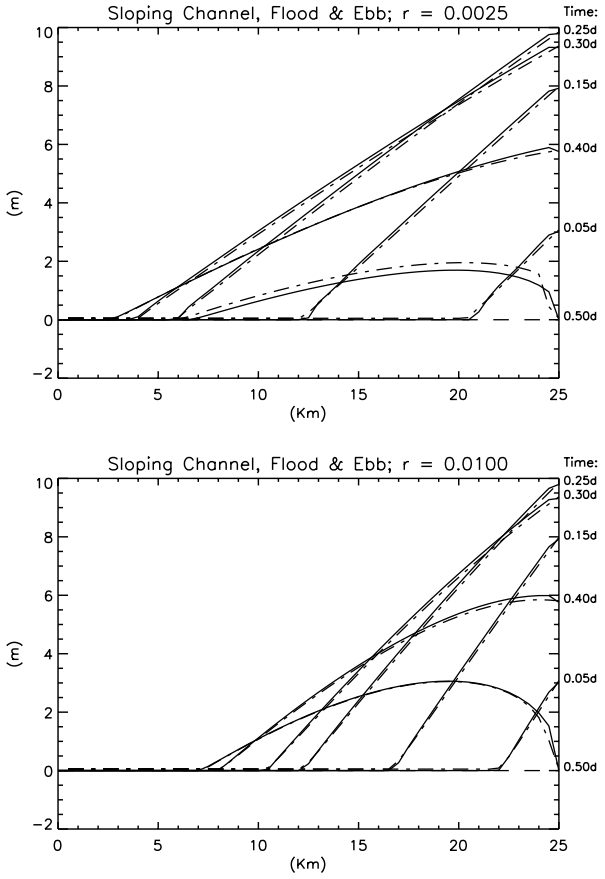

Fig. 7. Comparison of the flooding (wetting) and ebbing (drying) POM-WAD simulation (dash-dot) in a channel with linear sloping bottom topography with the solution from the advective-diffusion equation (solid). Upper panel is for $r = 2.5 \times 10^{-3}$ m s^{-1} and lower panel for $r = 10^{-2}$ m s^{-1}. Plotted are water depths D at the indicated times.

3.4. A channel with a step bottom

We now show a case in which the channel is flat $H = 1.5$ m for $0 \leqslant x \leqslant 19$ km, then it slopes down over a smooth step to a deeper portion seaward of which (at $x = L = 25$ km, where $H = 4$ m) sea level is specified (Fig. 8). The specification is flood for the first 0.25 day, ebb for the next 0.25 day (i.e. $D_0 = 4$ m and $n = 1$ in Eq. (11)), but then D is kept $= 0$ for the remaining

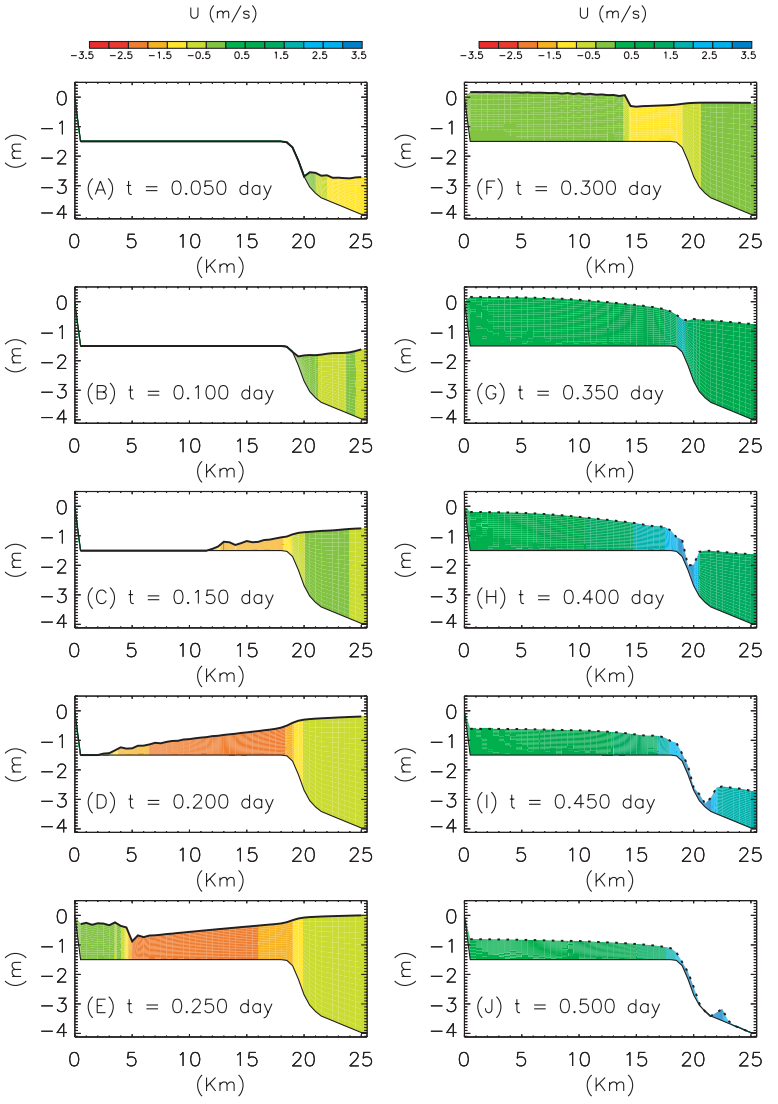

Fig. 8. Flooding (wetting) and ebbing (drying) POM-WAD simulation in a channel with a step bottom topography, closed at left ($x = 0$) and open at right ($x = L = 25$ km) where water depth D increases to a maximum of 4 m for the first 0.25 day period, and falls to 0 for the next 0.25 days, at the end of which D is kept zero. Shown are water level and velocity (in color scale in m/s given on top) at the indicated times. Left panels (A–E) are flood and right panels (F–J) are ebb. The friction coefficient $r = 0$ m/s.

integration of 4.5 more days. Fig. 8 shows the inviscid result in terms of water level and velocity (colored) at the ten indicated times over the first 0.5 day. As water floods over the step (Fig. 8A and B), a bore is produced intruding landward over the dry channel at a speed of about 2 m s^{-1} (Fig. 8C and D). POM-WAD works well in this case as the wetting intrusion occurs with little 'wiggles' or 'irregularities' that may be associated with such strong currents. Upon reaching the left-hand wall ($x = 0$), pile-up of fluid occurs and a reflected wave is produced (Fig. 8E and F). As

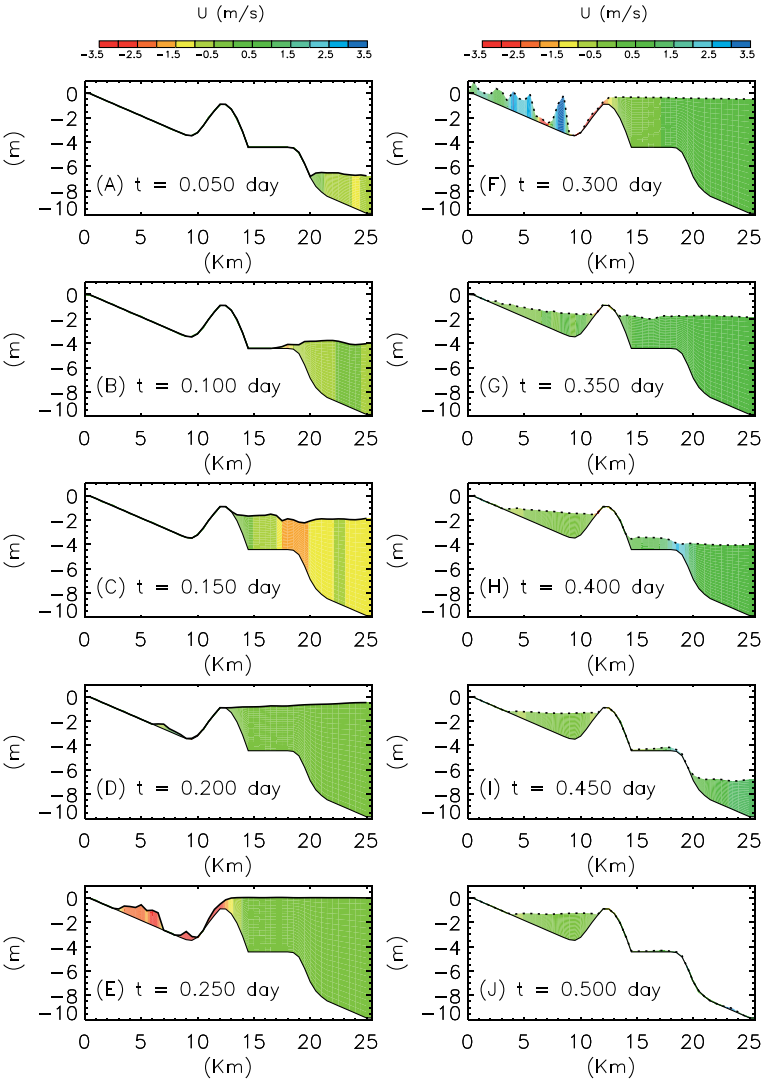

Fig. 9. Flooding (wetting) and ebbing (drying) POM-WAD simulation in a channel with a step, a bump and a bowl-shaped bottom topography, closed at left ($x = 0$) and open at right ($x = L = 25$ km) where water depth D increases to a maximum of 10 m for the first 0.25 day period, and falls to 0 for the next 0.25 days, at the end of which D is kept zero. Shown are water level and velocity (in color scale in m/s given on top) at the indicated times. Left panels (A–E) are flood and right panels (F–J) are ebb. The friction coefficient $r = 0$ m/s.

the sea-side water level falls, ebb speed over the step becomes very strong, $\overline{U} = 3\ \mathrm{m\,s^{-1}}$, and flow becomes supercritical, $\overline{U}/(gD)^{1/2} \approx 1.3$ (Fig. 8H). A hydraulic jump develops as flow adjusts to become sub-critical down the step. Also, because of the different water depths, the response time scale is shorter on the seaward side of the step than it is on the shallow side. Passage of the jump and faster falling of the sea-side water level leave the step and slope with only a thin film of fluid through which fluid on the shallow side of the step drains down-slope. Draining occurs in the form of down-slope bursts of fluid (Fig. 8J). The shallow fluid drains completely in 1.5 days (not shown), which is slow in comparison to the ebbing time of the linear-slope case.

In the frictional case (not shown), no bore intrusion develops. Instead, flood on the shallow side of the step proceeds more slowly, and water level decreases linearly from the sea to the intrusion nose, exactly as that predicted by the solution discussed earlier for Fig. 4b (see the curves for $t \leqslant 0.5$ for $r = 10^{-3}\ \mathrm{m\,s^{-1}}$, or $t \leqslant 1$ for $r = 2.5 \times 10^{-3}\ \mathrm{m\,s^{-1}}$). During ebb, flow over the step does not become supercritical. Water level on the seaward side again falls faster (because of different response time scales), and the step and slope are again left with a thin film of fluid through which fluid drains. The draining is slower and smoother than the inviscid case: it now takes 4 days to drain completely. Weak down-slope 'jumps' and 'bursts' do occur as breaking-wave solution develops due to topographic curvature effect in the 'advective' term of Eq. (7). The solution over the shallow side of the step follows closely that shown in Fig. 4a.

3.5. A channel with a step, a bump and a bowl-shaped bottom

Fig. 9 shows flooding and ebbing in a channel with a step, a bump and a bowl-shaped bottom at the indicated times. As in Fig. 8, water-level specification at $x = L$ is flood for the first 0.25 day, ebb for the next 0.25 day (i.e. $D_0 = 10$ m and $n = 1$ in Eq. (11)), but then D is kept $= 0$ for the remaining integration of 4.5 more days. Flooding occurs over the step in much the same way as that shown in Fig. 8. Near the flood peak ($t \approx 0.2$ day, Fig. 9D), water begins to spill over the bump. The spill occurs as flow becomes supercritical, with $\overline{U} \approx -3\ \mathrm{m\,s^{-1}}$, in a thin layer down the bump into the bowl. Bore intrusion occurs up the slope towards the left wall (Fig. 9E), then fluid sloshes back and forth in the bowl (Fig. 9F–I) as water seaward of the bump ebbs, and comes to equilibrium with a pool of water left in the bowl at the end (Fig. 9J). The solution with friction is similar except again the flow is smoother (not shown).

4. A two-dimensional wetting example: comparison with laboratory experiment

We have also tested POM-WAD against one of the two dam-break problems simulated in the laboratory by Stelling and Duinmeijer (2003). The experiment set-up consists of two reservoirs, A and B, separated by a wall in the middle of which is a gate of width 0.4 m that can be lifted (Fig. 10). Reservoir B is initially filled with water of height 0.6 m. In Stelling and Duinmeijer's first experiment, reservoir A is initially dry, and in another it contains a thin film of water 0.05 m in thickness. The gate is then lifted with a speed of 0.16 m/s and the subsequent flooding in reservoir A is studied. Since POM-WAD requires a non-zero water depth, only the second experiment with initially wet bed in reservoir A is tested. The simulation period is 30 s.

This is a very stringent test case for a WAD scheme. As detailed in Stelling and Duinmeijer (2003), the ensuing flow after the gate is lifted consists of rapid expansion, then formation of

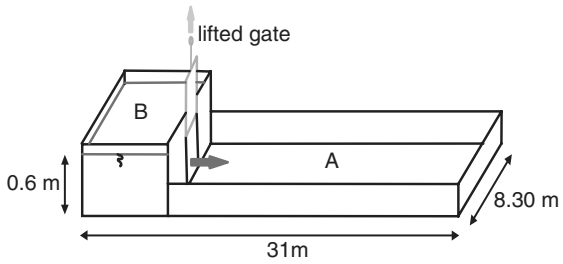

Fig. 10. Laboratory experimental set-up for the dam-break problem; from Stelling and Duinmeijer (2003).

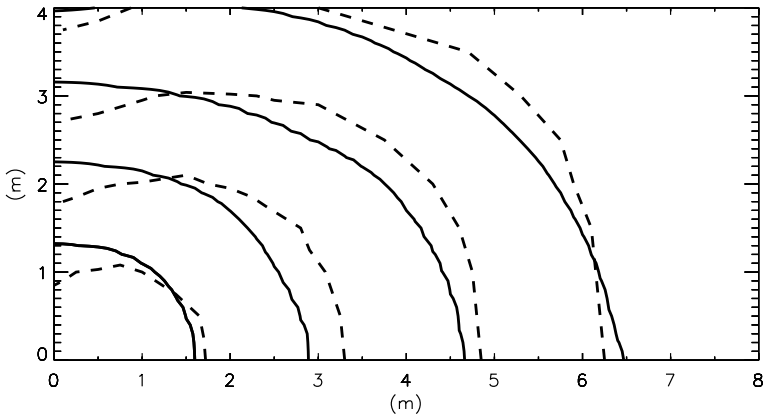

Fig. 11. POM-WAD simulation of the dam-break experiment of Stelling and Duinmeijer (2003). Curves indicate bore fronts at $t = 1$, 2, 3 and 4 s after the gate is lifted. Because of symmetry, only half of the domain in reservoir A (Fig. 10) is shown. Solid is POM-WAD solution and dash is laboratory data. The friction coefficient $r = 2.5 \times 10^{-3}$ m/s.

hydraulic jump that propagates outward from the gate. Stelling and Duinmeijer (2003) devised clever schemes that conserve mass as well as guarantee non-negative water levels and correct momentum and head balance near discontinuities. The original POM-WAD yielded excessive oscillations for this problem and became unstable after $t > 12$ s. We therefore modify the scheme and use Smolarkiewicz (1984) positive-definite advection scheme to solve the water-level equation; other aspects of the WAD algorithm are not changed. The resulting scheme is stable. Fig. 11 shows the bore fronts at $t = 1$, 2, 3 and 4 s after the gate is lifted. Because of symmetry, only half of the domain in reservoir A is shown. Solid is the POM-WAD solution and this is compared with the laboratory data in dashed curves. Reasonable agreements between the two can be seen. The velocities (not shown) in this case exceed 2–3 m/s. The friction coefficient $r = 2.5 \times 10^{-3}$ m/s but the solution is not sensitive to this value (cf. Stelling and Duinmeijer, 2003).

5. Conclusions

A wetting and drying (WAD) scheme has been implemented into the Princeton Ocean Model (POM). To check the new algorithm and its accuracy, POM-WAD is tested for simple flood and

ebb cases in one-dimensional channels, as well as for a two-dimensional dam-break problem in the laboratory. The shallow-water system is shown to admit a well-defined 'dry' solution for which the total water depth D can be zero in the limit of moderate bottom friction and small topographic variations. A non-linear diffusion equation then results, with an effective diffusivity that varies like D^2, so that 'dry' cells are regions where 'diffusion' is very small. For more general topography, D is governed by a Burger's type advection–diffusion equation with a source term, for which breaking-wave solutions can develop even when momentum advection is neglected. The solutions to these simpler equations provide the basis for checking the accuracy and interpretations of the solutions obtained from POM-WAD.

The laboratory dam-break problem is a stringent test for any WAD scheme. The flow involves rapid expansion and propagating bores. Here, a positive-definite advection scheme for D is found to work well with POM-WAD. Reasonable agreements between the modeled and experimental positions of the bore fronts are obtained.

We have also tested POM-WAD in other two-dimensional and fully three-dimensional (with friction) cases with more complicated bottom topography and basin geometry. The results are not shown here as there are no data against which we can check the solutions in these more complicated cases. Suffice it to state here that the algorithm appears to be robust. Future work will be to use POM-WAD to simulate the strong tides that occur in the Cook Inlet, Alaska, where modeled WAD can then be compared with observations. I should mention also that the sigma-coordinate used in POM makes it relatively easy to extend the proposed WAD algorithm to three dimensions, since vertical cells are either wet or dry in sigma-coordinate. This is important since, as stated earlier, our goal is to merge WAD with existing POM numerics that handle open-ocean processes. A cautionary note: similar to the two-dimensional case, the difficulty we may encounter in three dimensions is strong non-linearity due to fronts and propagating bores, say those relating to buoyant outflows from rivers (c.f. Stelling and Duinmeijer, 2003).

Acknowledgements

Comments from two anonymous reviewers greatly improve the manuscript. This study is supported by the Minerals Management Service under contract # 0103CT72021. Computing was conducted at GFDL/NOAA.

Appendix A

By invoking condition (5), the following two-dimensional equation for D results:

$$\frac{\partial D}{\partial t} \approx \frac{\partial}{\partial x}\left\{\frac{(gD^2/r)}{(1+F^2)}\left(\frac{\partial(D-H)}{\partial x}+F\frac{\partial(D-H)}{\partial y}\right)\right\}+\frac{\partial}{\partial y}\left\{\frac{(gD^2/r)}{(1+F^2)}\left(\frac{\partial(D-H)}{\partial y}-F\frac{\partial(D-H)}{\partial x}\right)\right\}, \tag{A.1}$$

where $F = Df/r$, and f is the Coriolis parameter. With $F = 0$ and $|\nabla D| \gg |\nabla H|$, we again obtain a non-linear diffusion equation (in two dimensions), which with appropriate boundary and initial

conditions would again admit drying $D = 0$ as a solution. For more general topography, other similarities with the one-dimensional case may also be inferred. One notes also that for common values of f and r, the Coriolis cannot be neglected. Its effects in large-scale flooding and ebbing are therefore likely to yield some interesting WAD processes.

References

Balzano, A., 1998. Evaluation of methods for numerical simulation of wetting and drying in shallow water flow models. Coastal Eng. 34, 83–107.

Carslaw, H.S., Jaeger, J.C., 1959. Conduction of Heat in Solids, second ed. Oxford University Press. 510pp.

Casulli, V., Cheng, R., 1992. Semi-implicit finite difference methods for three-dimensional shallow water flow. Int. J. Numer. Methods Fluids 15, 629–648.

Ezer, T., Oey, L.-Y., Sturges, W., Lee, H.-C., 2003. The variability of currents in the Yucatan Channel: analysis of results from a numerical ocean model. J. Geophys. Res. Available from <10.1029/2002JC001509>.

Fan, S.J., Oey, L.-Y., Hamilton, P., 2004. Assimilation of drifters and satellite data in a circulation model of the northeastern Gulf of Mexico. Cont. Shelf Res. 24, 1001–1013.

Flather, R.A., Hubbert, K.P., 1990. Tide and surge models for shallow-water—Morecambe Bay revisited. In: Davies, A.M. (Ed.), Modeling Marine Systems, vol. I. CRC Press, pp. 135–166.

Ji, Z.G., Morton, M.R., Hamrick, J.M., 2001. Wetting and drying simulation of estuarine processes. Estuarine Coastal Shelf Sci. 53, 683–700.

Mellor, G.L., 2002. Users' Guide for a Three-Dimensional, Prim-Itive Equation, Numerical Ocean Model (July 2002 version). Program in Atmospheric and Oceanic Sciences. Princeton University. 42pp.

Mellor, G.L., 2003. The three dimensional, current and surface wave equations. J. Phys. Oceanogr. 33, 1978–1989.

Oey, L.-Y., 1996. Simulation of mesoscale variability in the Gulf of Mexico. J. Phys. Oceanogr. 26, 145–175.

Oey, L.-Y., Lee, H.-C., 2002. Deep eddy energy and topographic Rossby waves in the Gulf of Mexico. J. Phys. Oceanogr. 32, 3499–3527.

Oey, L.-Y., Zhang, H.-C., in press. A mechanism for the generation of subsurface cyclones and jets. Cont. Shelf Res. Available from <http://www.aos.princeton.edu/WWWPUBLIC/PROFS/>.

Oey, L.-Y., Mellor, G.L., Hires, R.I., 1985. A three-dimensional simulation of the Hudson–Raritan estuary. Part I: Description of the model and model simulations. J. Phys. Oceanogr. 15, 1676–1692.

Oey, L.-Y., Lee, H.-C., Schmitz Jr., W.J., 2003. Effects of winds and Caribbean eddies on the frequency of loop current eddy shedding: a numerical model study. J. Geophys. Res. 108 (C1O), 3324. Available from <doi:10.1029/2002JC001698>.

Oey, L.-Y., Winnant, C., Dever, E., Johnson, W., Wang, D.-P., 2004. A model of the near-surface circulation of the Santa Barbara Channel: comparison with observations and dynamical interpretations. J. Phys. Oceangr. 34, 23–43.

Proudman, J., 1953. Dynamic Oceanography. Methuen, John Wiley & Sons, London, New York. 409pp.

Richtmyer, R.D., Morton, K.W., 1957. Difference Methods for Initial-Value Problems. Interscience Publishers, John Wiley & Sons, New York. 405pp.

Smolarkiewicz, P.K., 1984. A fully multidimensional positive definite advection transport algorithm with small implicit diffusion. J. Comput. Phys. 54, 325–362.

Stelling, G.S., Wiersma, A.K., Willemse, J.B.T.M., 1986. Practical aspects of accurate tidal computations. J. ASCE Hydraul. Eng. 9, 802–817.

Stelling, G.S., Duinmeijer, S.P.A., 2003. A staggered conservative scheme for every Froude number in rapidly varied shallow water flows. Int. J. Numer. Meth. Fluids 43, 1329–1354.

Wang, D.-P., Oey, L.-Y., Ezer, T., Hamilton, P., 2003. Nearsurface currents in DeSoto Canyon. J. Phys. Oceanogr. 33, 313–326.